CHAPTER 3: Modelling of Sloshing

3.1 Introduction

This chapter details the modelling methods used for the sloshing event. A description of the automated grid generation procedure and related issues is provided. An overview of the validation procedures follows and an analysis of the results from the validation within the context of the sloshing modelling will conclude the chapter. The aim of this chapter is to determine the feasibility of using CFD to evaluate sloshing performance as part of a liquid container design cycle.

3.2 Computational Fluid Dynamics

Due to availability, the commercial CFD code Fluent v6.x [19] is used throughout the study for the modelling of the sloshing event. Fluent's grid generator or pre-processor is Gambit, and the section that follows provides a description of the automated use of this pre-processor. Automation of the pre-processor is necessary for the optimisation procedures that follow in chapters 4 and 6.

3.2.1 Grid Generation

Once the geometry and topology of a tank and its damping devices are established, it is necessary to recreate the fluid domain in the pre-processor. In three dimensions, the damping devices may include baffles with holes, or as in reference 14 vertical cylinders. In two dimensions, one can only consider horizontal circles or baffles with or without slots. Figure 3.1 and Figure 3.2 illustrate typical 3D and 2D geometries encountered during this study, respectively. In the context of CFD, it is always advantageous to simplify a given geometry, in that it will reduce computational expense. To simplify the 3D geometry, a symmetry plane can be defined as illustrated in Figure 3.1. 3D geometries may in turn be further simplified to 2D, although features like holes can no longer be captured and side wall effects will also not be

modelled. 2D geometries are intuitively computationally less expensive, however in all CFD analyses one must be wary of over-simplifying geometry to the point where the analysis is no longer meaningful.

Figure 3.1 shows a section through the mesh of the 3D geometry, comprised of hexahedral cells only. Although the CFD code is capable of handling tetrahedral cells, accuracy and solution times when using hexahedral cells are far superior. Hexahedral cells in the circular holes are achieved by using an iron-cross formation, that subdivides the circle into five four-sided sections. The 2D geometry is far simpler from the perspective of meshing since it easily lends itself to a fully-structured Cartesian mesh. The implication of 3D versus 2D can be best appreciated when one considers that a typical 3D sloshing analysis will take approximately 48 hours (400 000 cells), while a 2D analysis will take approximate 4 hours (25 000 cells) for the same period of real time solved on the same computer (2GHz P4 Linux workstation). All operations in Gambit can be performed in a command line and in turn through a journal file that when executed will automatically generate the mesh. Appendix A provides a sample 2D journal file.

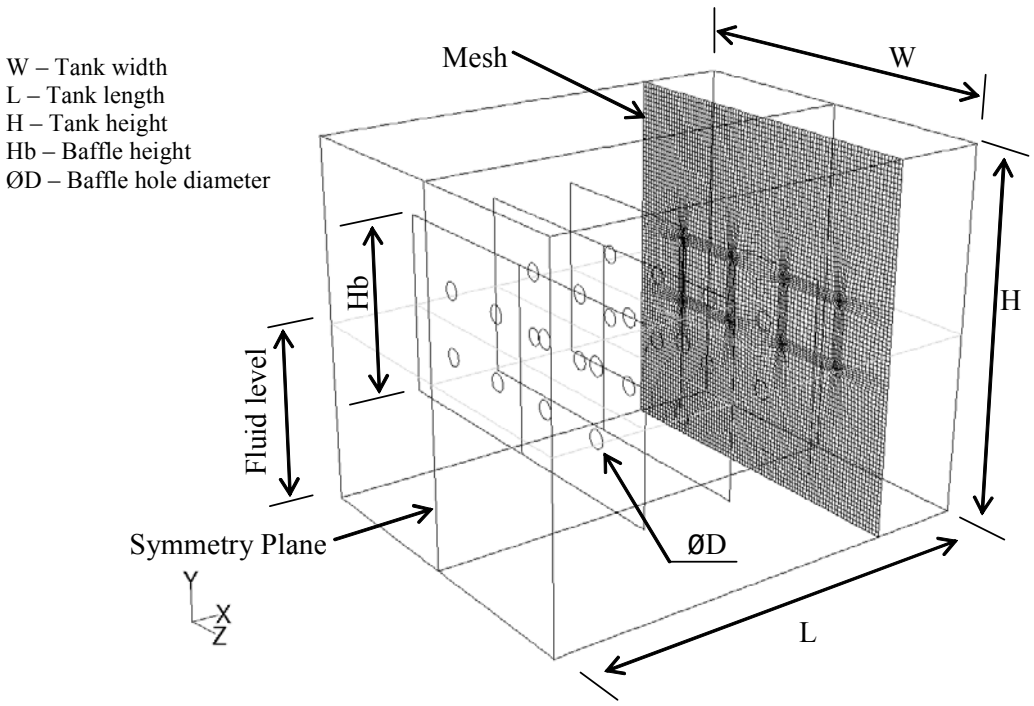

Figure 3.1: Typical 3D geometry and mesh

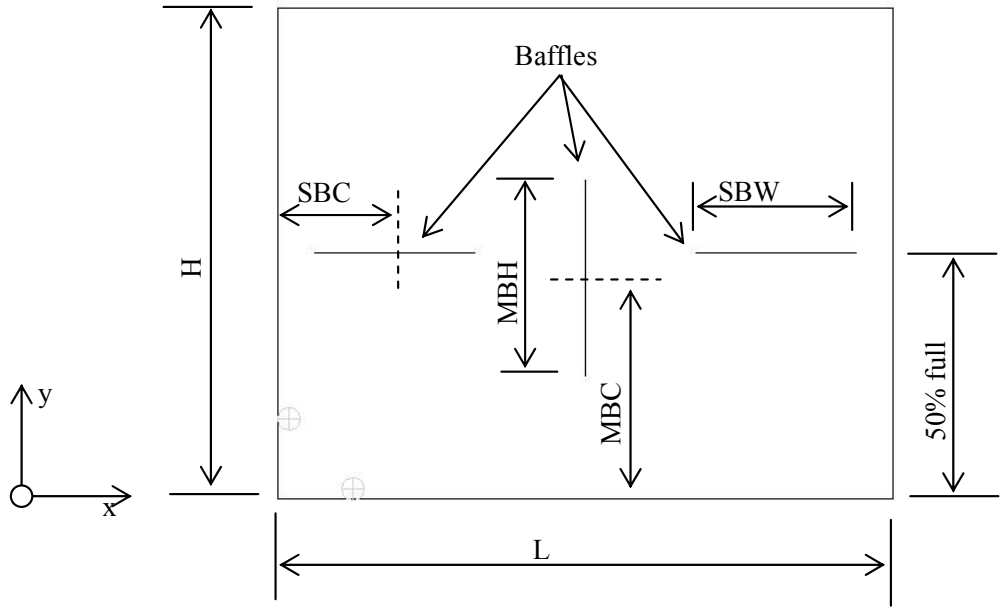

H – Tank height
L – Tank length
SBC – Side baffle centroid
SBW – Side baffle width
MBH – Mid baffle height
MBC – Mid baffle centroid

Figure 3.2: Typical 2D geometry

3.2.2 CFD Model Setup

Once the mesh has been generated in Gambit, it can be exported as a mesh file and imported into the CFD code Fluent. At this point the model must be scaled and set up for the flow assumptions that are appropriate for the case. This section will describe the number of settings that are used in the CFD model and where appropriate discuss the implications of the assumptions made.

Firstly, this type of analysis is transient and therefore requires an unsteady formulation of the CFD model. Unsteady simulations are traditionally more time consuming and require that a time step size be provided. The time step size must be sufficiently small to ensure the stability of the code and a time-accurate solution. Typical values for this study range from 1 to 2.5 ms and usually equates to

approximately 10 sub-iterations per time step for stability in the solution of the most non-linear wave motions.

Since the liquid container is partially filled, two phases exist in the flow field, liquid and gas. The Volume of Fluid (Section 2.4.3.4) model is used to monitor the motion of the free surface. This model is commonly used for the modelling of sloshing [31]. The formulation is simple and relatively inexpensive, and provides good results in cases that involve large free surfaces. All material properties and conservation equations are altered to consider all terms as volume fraction weighted summations. Within the solver, once the flow field has been initialised with liquid throughout, a region is defined that corresponds to the initial location of the gaseous phase. A volume fraction of unity for the gas is then patched over this region.

In this study, the two phases are water and air. Since there is a free surface, surface tension must also be considered for the water-air interface. The surface tension coefficient (γ) was considered to be 0.073N/m at 20˚C [50].

Since the case in study has no inlet or outlet boundaries, a load curve is used as a user-defined boundary condition. An acceleration curve is imposed on the model in the form of a momentum source term. A user-defined c-code converts acceleration data into momentum source (see Section 2.4.3.2) for the *i*-th cell through the formulation given in equation 3.1 below (illustrates formation for *x*-direction), where S_i^m is the momentum source for the *i*-th cell, *x* is displacement in the local *x*-direction, *t* is real time, and ρ is the volume fraction weighted density in the *i*-th grid cell. Appendix B provides a sample c-code that would do this conversion if provided with a text file containing an acceleration versus time signal as two columns of data.

$$S_i^m = \frac{\partial x}{\partial t}\rho_i \tag{3.1}$$

As in references 31 and 51, turbulence is considered very low and if transitional flow exists, it is confined to short duration, small region events. For this reason, it is considered more appropriate to assume a laminar flow field. The validation section of this chapter illustrates the difference in results when assuming turbulent flow. It is

important to remember that when assuming turbulent flow, the viscosity within the Navier-Stokes formulation will increase in all cells, including those involved in strictly laminar flow (See Section 2.4.3.4).

As with the pre-processor Gambit, all settings and commands can be done through a text user interface. A sample journal file that sets up the 2D CFD run can be seen in Appendix C.

3.3 Experimental Validation

Since a major part of this study revolves around the utilisation of CFD as a technique to model sloshing, it would be appropriate to perform some level of validation. The aim of the validation is to evaluate the overall performance of the CFD code with its chosen settings, as a tool to determine the level of sloshing in a liquid container.

3.3.1 Experimental Setup

The experimental modelling is divided into two phases. The first and preliminary phase involved a small Perspex or Plexiglass container (H = 200mm, W = 200mm, L = 250mm), mounted on a set of inclined rails. The second phase was an extension of the first phase and involved a larger Perspex container (H = 400mm, W = 400mm, L = 500mm), mounted on the loading bed of a 1-ton truck. In both cases, a digital video camera was aligned with the side of the tank to monitor the motion of coloured water in the partially-filled container.

The Perspex tank for the first phase is seated horizontally on a trolley that runs down an inclined track (see Figure 3.3 below). The frame consists of a 5m-long double track, tracks 385mm apart, with a drop in elevation of 1.7m. The trolley is fitted with ball-bearing wheels and runs freely along the rail. Attached to both the front and rear of the trolley is a rope and shock cord. The shock cord represents a method of accelerating the trolley from standstill and decelerating it before it reaches the end of the rail. The single rope completes a cycle through four pulleys and runs in a one-way

cam cleat. The cam cleat is mounted rigidly to the frame and prevents the tank from moving back up the ramp under the force applied by the decelerating shock cord attached to the rear of the trolley. The idea is that the tank will accelerate down the rail, and then decelerate to a standstill as it comes into frame for the digital camera, mounted on a tripod, that is located near the end of the rail (See Figure 3.4). This will provide a digital video of the sloshing as the coloured water returns to its horizontal state of static equilibrium.

To link the experimental model with the CFD model in the context of the momentum source term as discussed in Section 3.2.2, an acceleration signal is measured on the Perspex tank. A 10.36mV/g Shear translational accelerometer and a PL202 analyser, shown in Figure 3.5, are used to measure the acceleration. The data are processed in Matlab v6 [52] and also involves the filtration through a low-pass Butterworth filter. The filtration at 5Hz is necessary to ensure the stability of the CFD code, when applying the signal as a load curve. Figure 3.6 below shows both the unfiltered raw data from the accelerometer (mV), and a filtered acceleration signal (m/s^2).

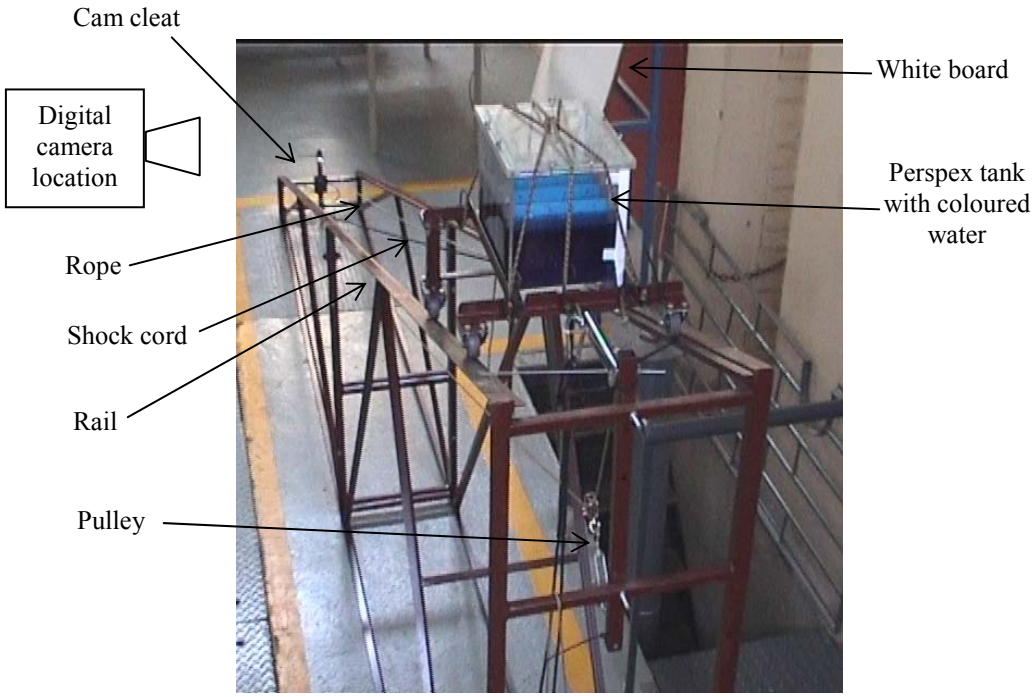

Figure 3.3: Phase 1 experimental setup

Figure 3.4: Location of camera at end of rail.

Figure 3.5: Acceleration measurement equipment

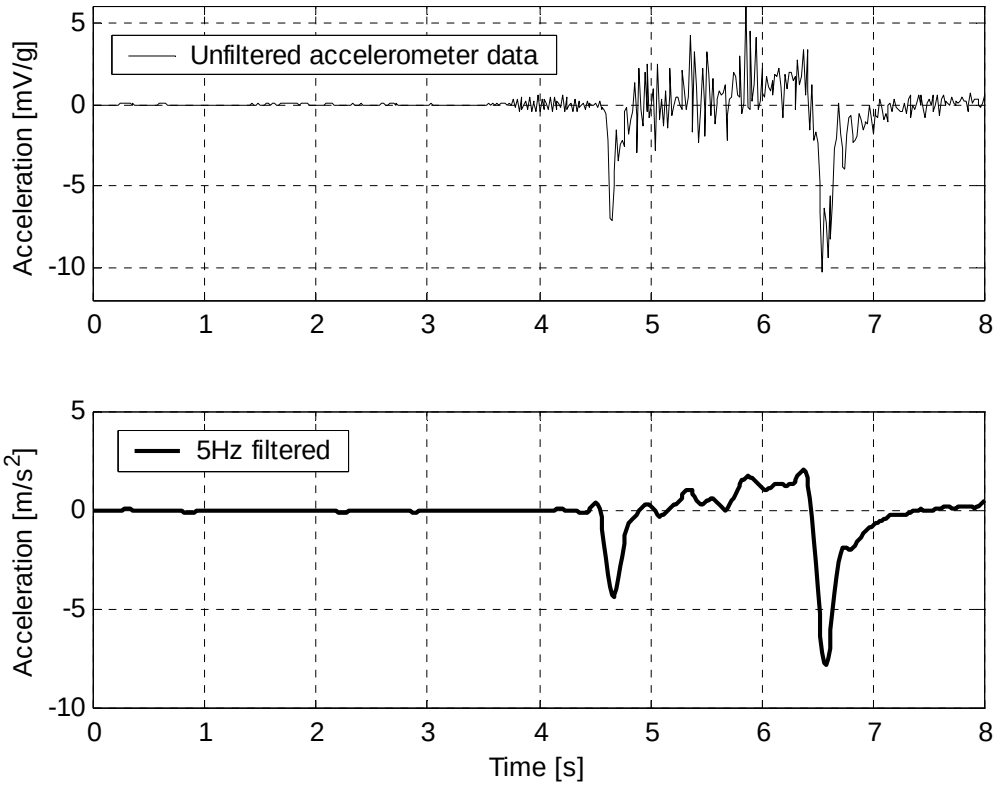

Figure 3.6: Acceleration data for experimental phase 1

It should be noted that although the filtered signal is significantly smoother, some signal detail and amplitude is lost as a consequence of filtration at this frequency.

The second phase of experimental modelling is an adaptation of the first phase to remedy some issues encountered. Figure 3.7 below provides a schematic representation of the setup as well as a digital photograph of the tank after instrumentation. Table 3.1 below gives an overview of the equipment used. The vehicle is accelerated from standstill to 40km/h and then decelerated back to standstill on a near-level tarmac road. The laptop stores both the pressure and acceleration data provided to it through its parallel port from the Spider data logger. The Spider data logger receives voltages on two serial ports, that represent the outputs from the accelerometer and the pressure sensor, both sampled at 100Hz. The pressure sensor is mounted at various points on the liquid container through holes drilled in the Perspex side walls. Both the pressure sensor and the accelerometer require dedicated and rated voltage supplies. The digital camera stores short videos of the motion of the fluid in the tank during the vehicle's acceleration and braking manoeuvre. Each configuration

of pressure sensor location and baffle setup is accompanied by its own video footage, acceleration data and pressure data, as it is impossible to exactly replicate the acceleration and braking manoeuvre.

The data from the laptop are further processed by converting the voltage data to m/s^2 and Pascal in the case of the acceleration and pressure data respectively. The processing is done in Matlab v6 [52] and also involves the filtration of the data through a low-pass Butterworth filter. However care must be taken not to remove too much content or amplitude, such that the CFD simulation will no longer adequately represents the test. Figure 3.8 illustrates the unfiltered data compared with data filtered at 1Hz and 5Hz for the phase-2 experimental setup. The unfiltered data is clearly very noisy and discontinuous, while the 1Hz filtered signal suffers from a loss of amplitude and detail. A filter frequency of 5Hz provided the best compromise in that it ensured a flat signal at the start of the test. Using the noisy signal in a CFD simulation caused bubbling and higher frequency sloshing that was not observed experimentally.

Table 3.1: Equipment used in phase-2 experimental setup

Equipment	Input	Output
Acer P1 laptop	220V and Parallel port	Stored CSV pressure and acceleration data
Spider 8-port data logger	220V and serial ports	Parallel port
Voltage Inverter	12V	220V
Sony Digital Video Camera	220V and image/light	Stored video footage
Shear 98mV/g Translational Accelerometer	9V	98mV/g and acceleration force
WIKA 100mBar diaphragm pressure sensor	20Vand induced pressure	4-20mA converted to 2-10V
2-channel Voltage supply	220V	20V (adjustable)
Accelerometer Power Supply	9V battery	-

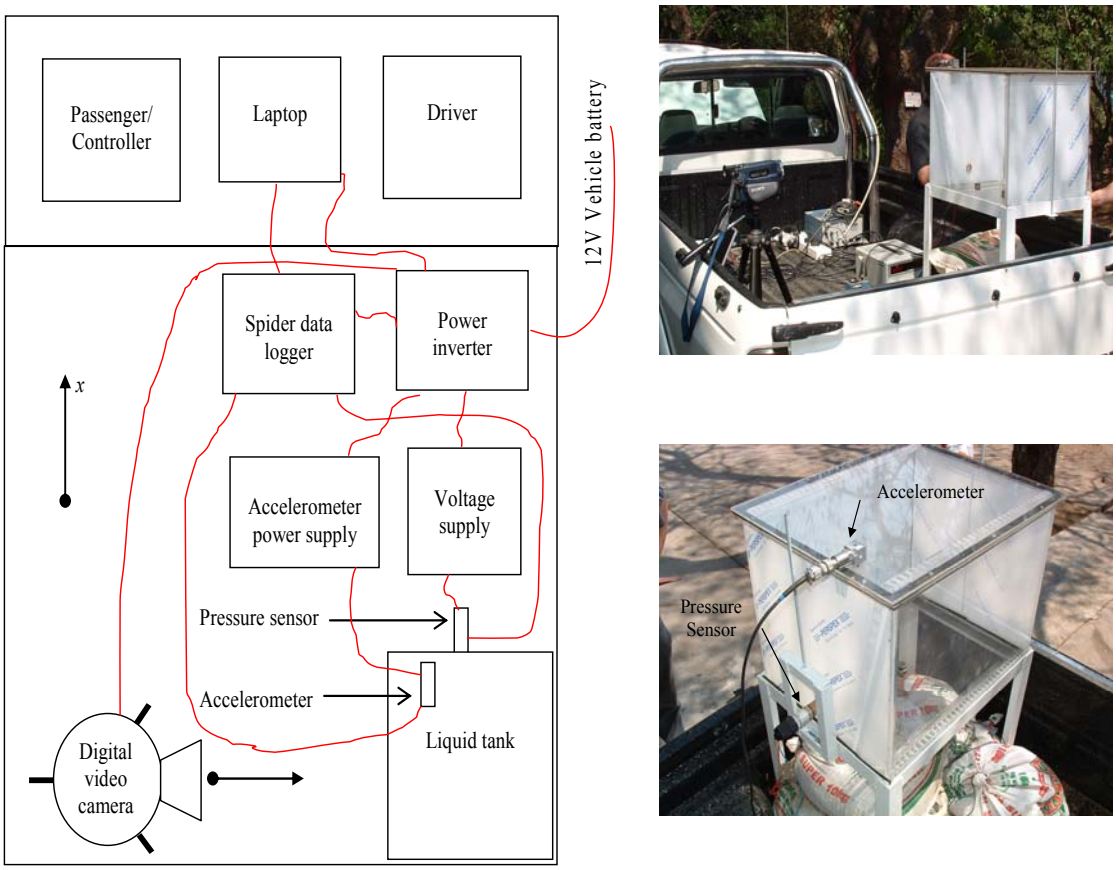

Figure 3.7: Phase-2 experimental setup

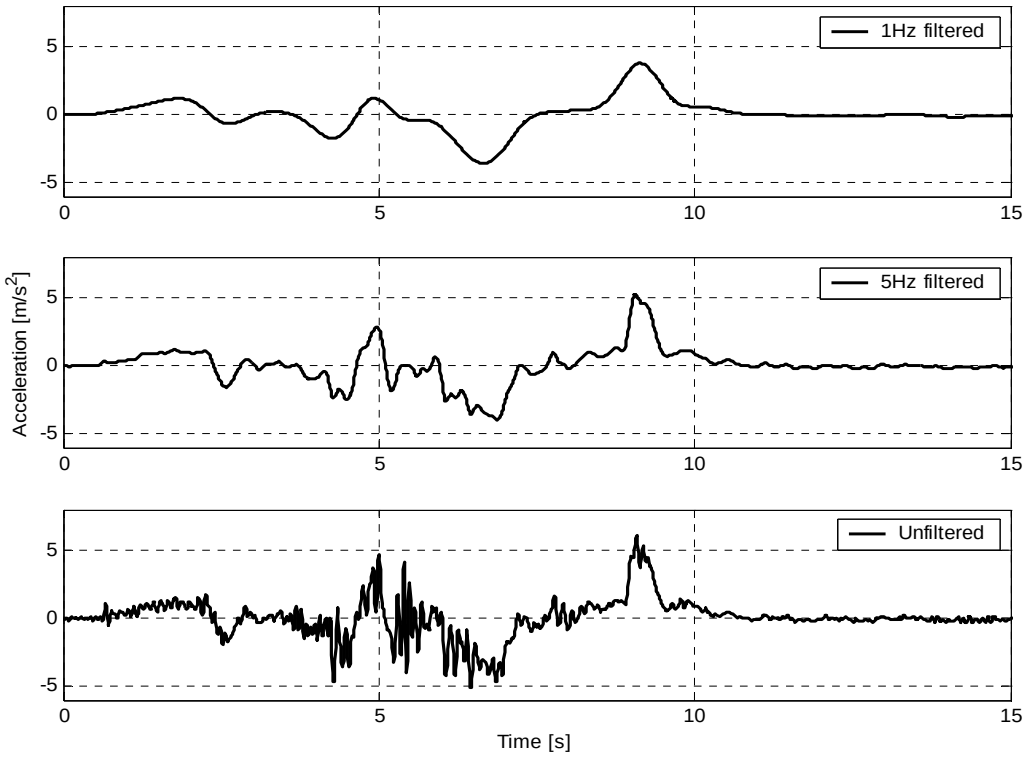

Figure 3.8: Acceleration curves for phase 2 experimental setup

The accelerometer used was supplied with a calibration certificate (Appendix D), and the WIKA pressure sensor was calibrated to static conditions. More detail on the calibration of pressure sensor can be seen in Appendix E.

3.3.2 Comparison of Results

This section provides the comparative results from the experimental and CFD models. The results presented are for both the 1st and 2nd phases of validation, with the second phase data providing qualitative and quantitative perspectives.

3.3.2.1 Phase 1 Experimental Validation

In order to validate the CFD results with the experimental setup, a computer model is recreated with the same dimensions and load curve as that measured in the experiment. This model is then solved, with digital image files created so that the computed wave nature can be compared to the experimental wave nature. The digital video clip taken during the experiment, showing the tank sloshing, can be linked to the acceleration curve at the time where the acceleration returns to zero. The frame rate of the video camera is 25 frames per second, giving a frame period of 0.04s. The video clip may now be viewed frame by frame and compared with the corresponding CFD results.

The first configuration considered is a baffled case with baffle height 80mm and hole diameter of 15mm (Hb = 80mm, ØD = 15mm in Figure 3.1). Figure 3.9 below shows the form of the tank with baffle as generated in Gambit. Figure 3.10 below shows a comparison of free-surface states for this baffled case. The CFD model is a 3D model with a symmetry plane as illustrated, and a laminar flow field assumption.

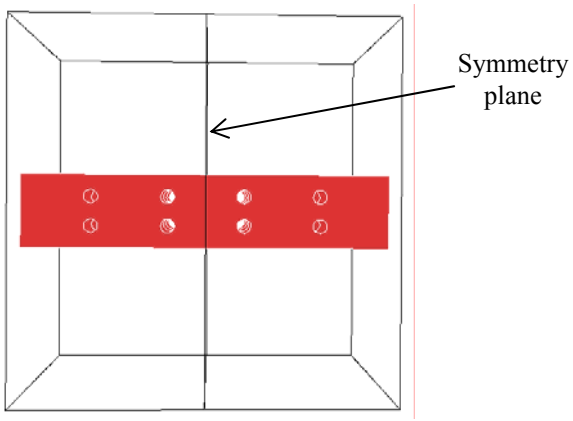

Figure 3.9: Baffled validation case (Hb = 80mm, D = Ø15mm)

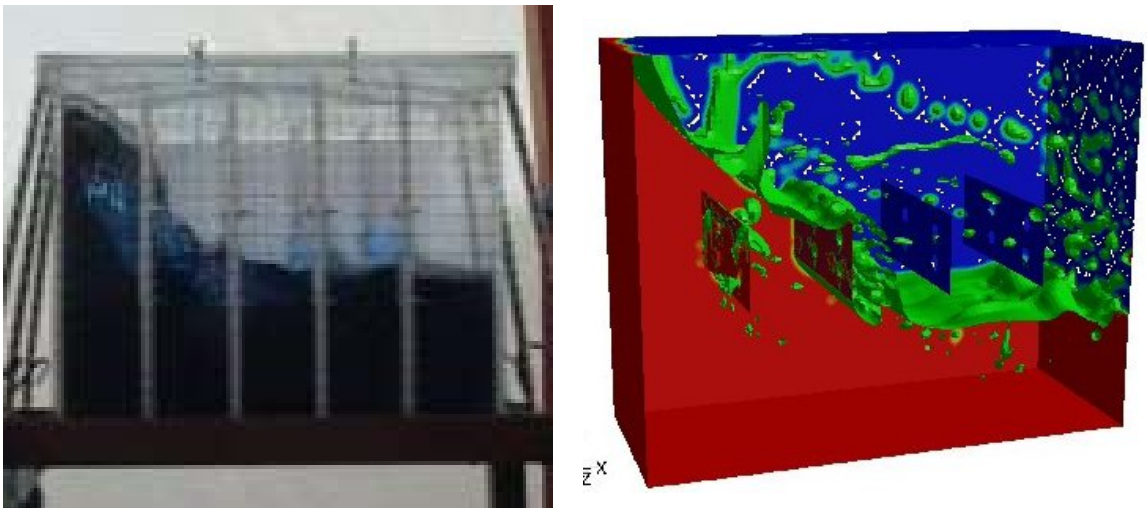

Figure 3.10: Sample of comparative free-surface states for baffled case (Experimental vs. CFD)

One can see that the CFD code is very capable of handling all the non-linearities of the sloshing, although the detail of the free surface is not correctly captured. However, the exact behaviour of all the splashes on the free surface is not repeatable and to try to match it would be futile.

Figure 3.11 below provides a frame for frame comparison of the wave motion for the baffled tank. The video camera provides an image of the coloured water that can be compared with a plot of contours of density from the CFD. As can be seen, the general wave motion and free surface behaviour is quite similar with some variations in amplitude. Variations in amplitude may be a result of the filtration of the

University of Pretoria etd – Kingsley, T C (2005)

acceleration signal as discussed in section 3.3.1. The general motion of the fluid is somewhat chaotic, in part due to the presence of the baffles. This chaotic nature of the wave motions makes it more difficult to make comparisons of definitive events during the sloshing.

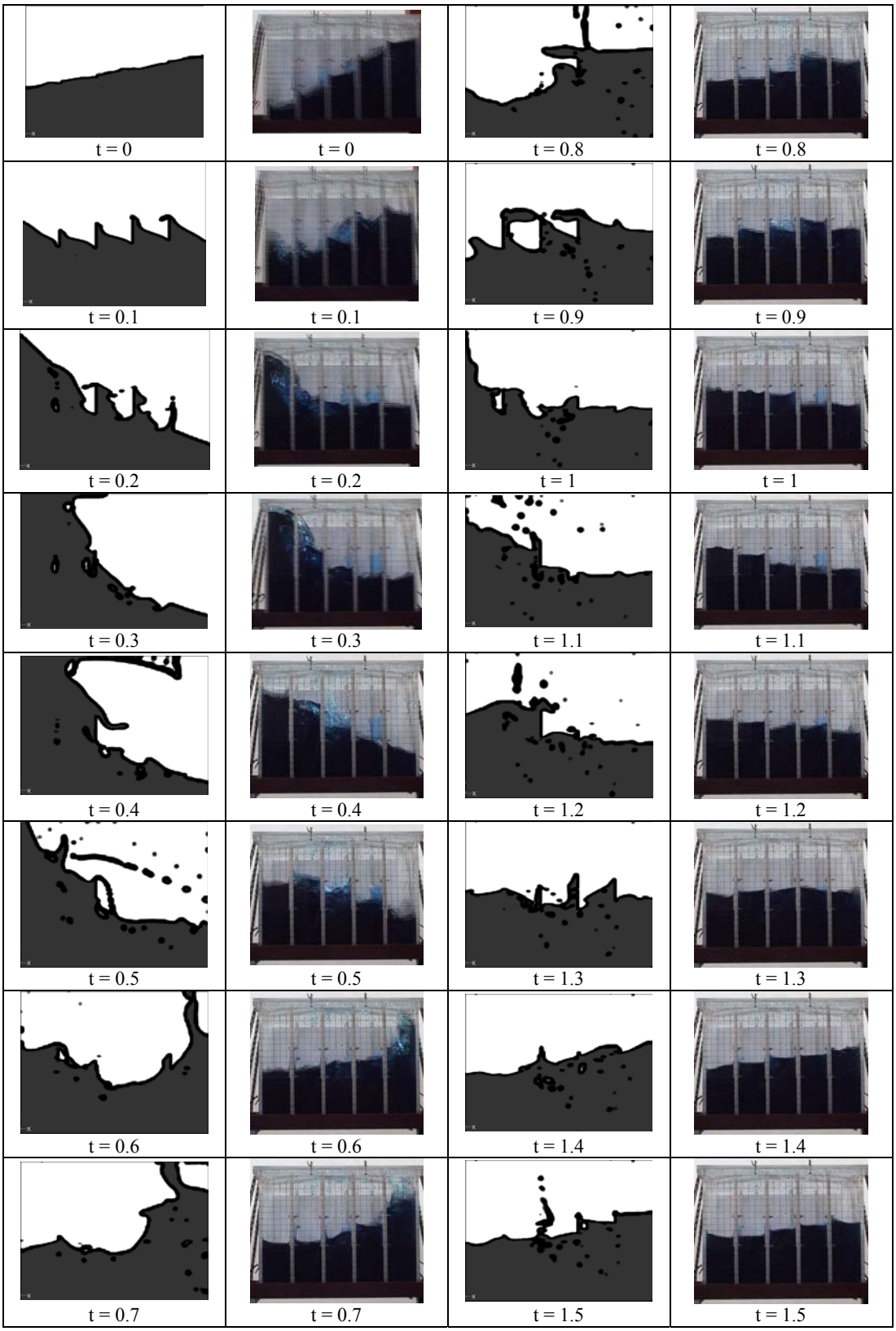

Figure 3.11: Wave comparison for baffled tank (LxWxH,Hb,ØD) = (250x200x200,80,15)mm: Experimental vs. CFD model at time, t [sec]

A further configuration considered is the same tank as above, but without any baffles. It is hoped that more definitive events may occur when there are no baffles to brake up the free surface. Figure 3.12 below illustrates a sample of a comparison of the free-surface states for the un-baffled case.

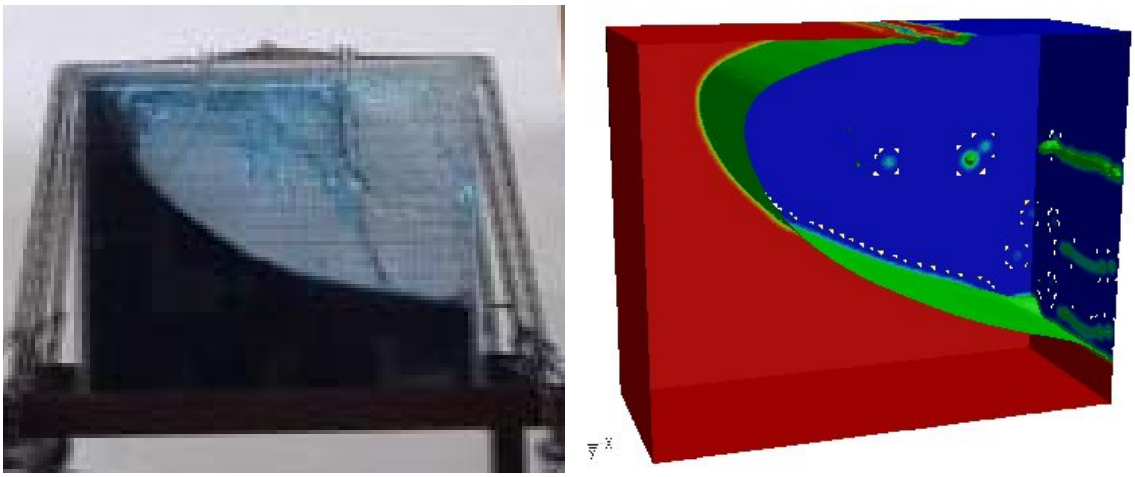

Figure 3.12: Sample of free surface states for un-baffled case (Experimental vs. CFD)

The laminar behaviour of the fluid on the roof of the container leads one to reconsider the laminar flow field assumption. This observation stimulated the consideration of a turbulence model for the validation. A first attempt at using a turbulence model involved the use of the k-ε model [19], however this did not provide results with any major difference to those seen in the laminar simulations. In particular, the separation of the fluid from the roof of the container when the free surface starts to fold over itself does not occur as soon as in the experimental model. A further model, Wilcox's k-ω model [20], is thought to predict earlier separation and provided slightly different results to the laminar simulations. Figure 3.13 below provides a frame-for-frame comparison of the un-baffled case for both laminar and turbulent assumptions. The t = 0.2sec frame clearly illustrates the earlier separation, however the same level of chaos in the free surface at the time of separation is still not evident. It is thought that the noisy three-dimensional loads experienced by the experimental model are what induce the additional chaos. Although the frames shown do not correspond exactly in time, they do exhibit similar wave forms. Discrepancies observed may be attributed to:

1. The cam cleat slips a different amount every run.
2. The CFD acceleration curve represents only one dimension of the accelerations felt by the experimental model.
3. The filtering process rounds the peaks of the signals, and so detail and amplitude is lost.
4. The baffle holders intrude into the flow and induce energy losses not included in the CFD model.
5. The flow field may experience some turbulence in certain areas but cannot be modelled as partially turbulent and partially laminar within the CFD model. As the VOF model does not support Large Eddy Simulations in Fluent, this factor cannot currently be evaluated.

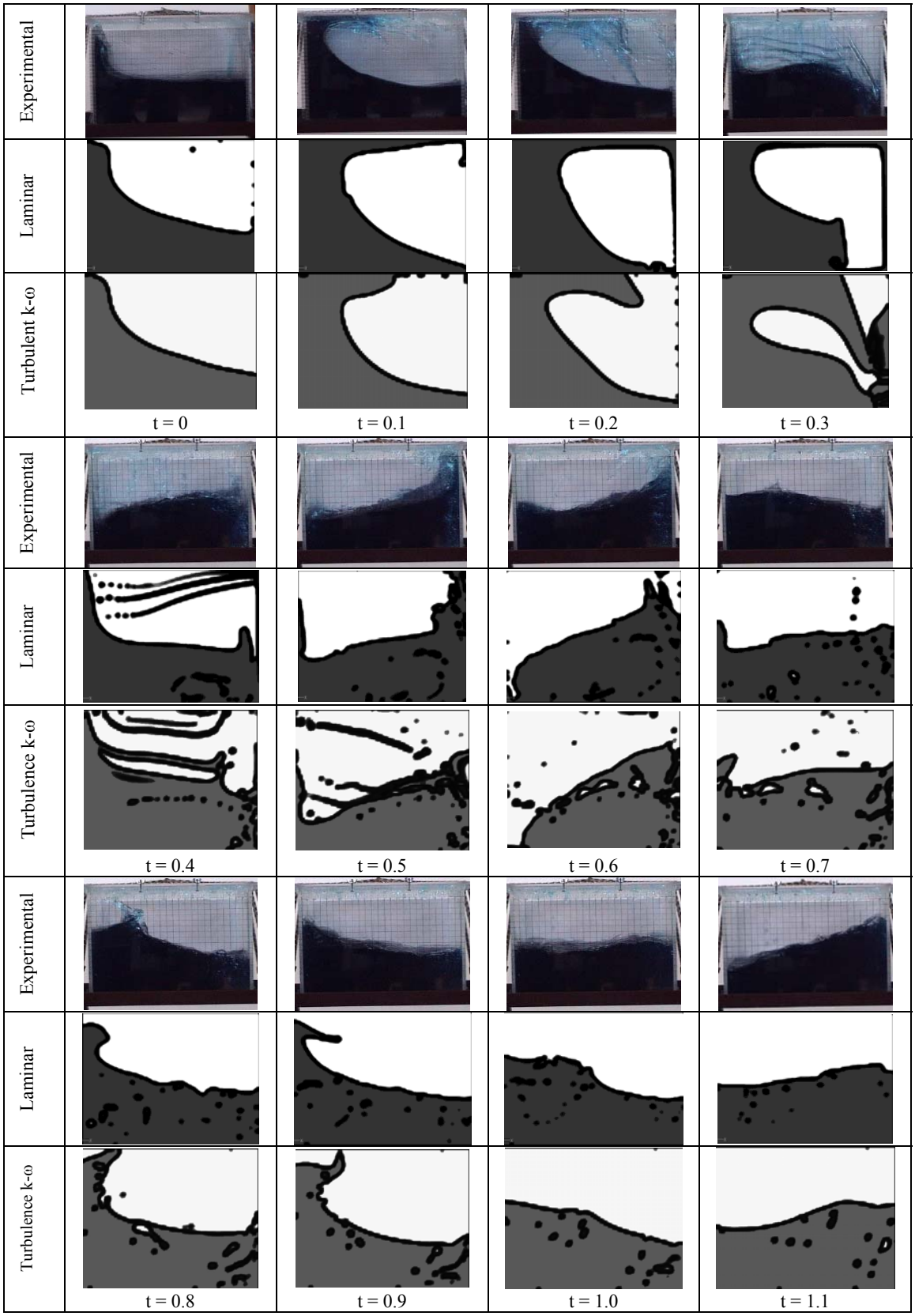

Figure 3.13: Wave comparison for an un-baffled case; Experiment, laminar flow and k-ω turbulence model at time, t [sec]: (LxWxH) = (250x200x200)mm

3.3.2.2 Phase 2 Experimental Validation

Phase two of the validation study attempts to improve the quality of the experimental setup used in phase one. The setup for phase two was discussed in section 3.3.1, but some of the major differences include:

1. An increased tank size to allow for pressure measurement and to reduce the effects of fittings inside the tank.
2. The experiment is done on the back of a truck so that the entire event can be analysed.
3. A pressure sensor is used to provide quantitative data.
4. Each run has a corresponding load curve since the motion of the vehicle is less repeatable than in phase 1.

The following section provides an overview of the comparative results for the phase 2 container (LxH; 500x400mm in Figure 3.2) with and without baffles. With reference to the phase 2 container, three pressure points are considered. Figure 3.14 indicates the location of the three pressure points (P1, P2 and P3) considered. All points are on the centre plane of the container. Since the different pressure points did not give much further insight, only pressure point 1 will be considered in the text for comparison.

Figure 3.15 shows a comparison of the liquid motion of the baffled and un-baffled cases for both the CFD and experimental model. The comparison is of frames from the digital video and a pressure contour plot in the liquid from the CFD simulations. The pressure contour plot provides us with additional data about the liquid phase that was not seen in the first validation phase. All frames are referenced to a specific sloshing event that occurs at the end the vehicle's deceleration. Points to take note of include the fact that experimental wave amplitudes are in general higher than CFD wave amplitudes, especially for baffled cases, although wave behaviour is quite similar. This may be a result of the filtering of the acceleration signal that does remove some peak accelerations, as can be seen in Figure 3.8 above. Disagreement is evident near in Figure 3.15 near 8 seconds. The figure illustrates the recovery of this disagreement as the low frequency acceleration experienced by the tank is reduced as

the vehicle comes to rest. The fluid motion that follows represents natural oscillatory modes and are thus unaffected by transient input signal. The final two slides show excellent agreement in this regime. The disagreement is confirmed in Figure 3.16 where further comparative data are provided in the form of gauge pressure curves extracted from the CFD and experimental setup and plotted over each other.

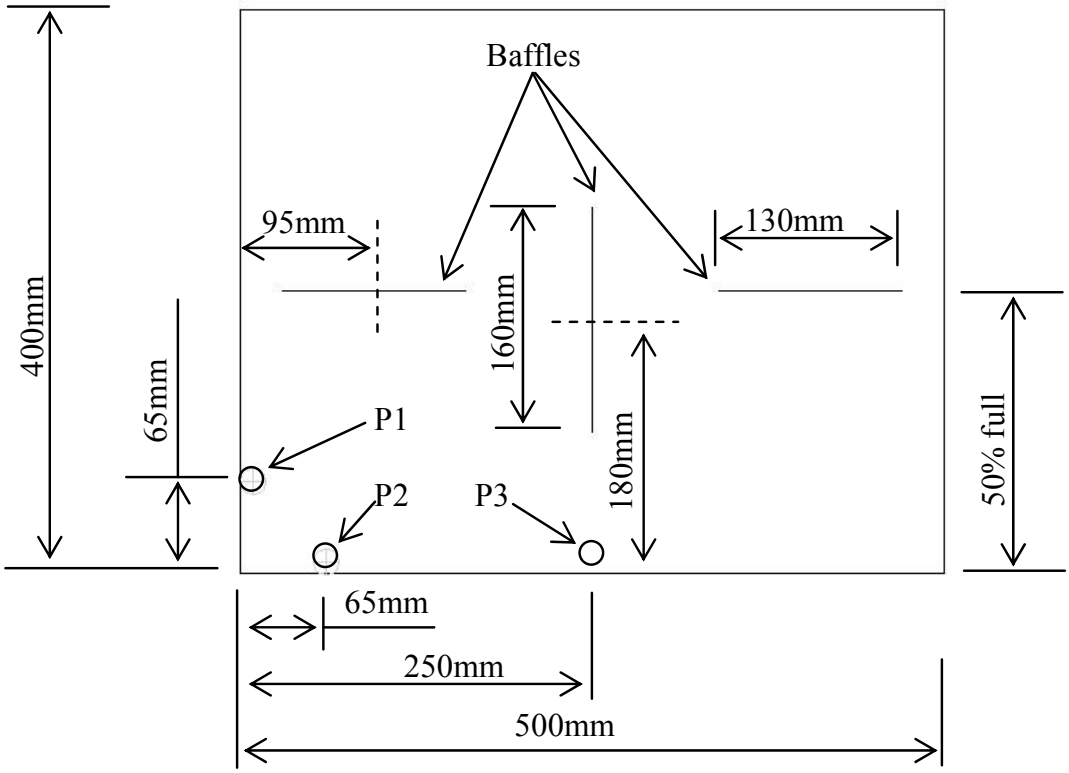

Figure 3.14: Configuration of phase two container and pressure point locations

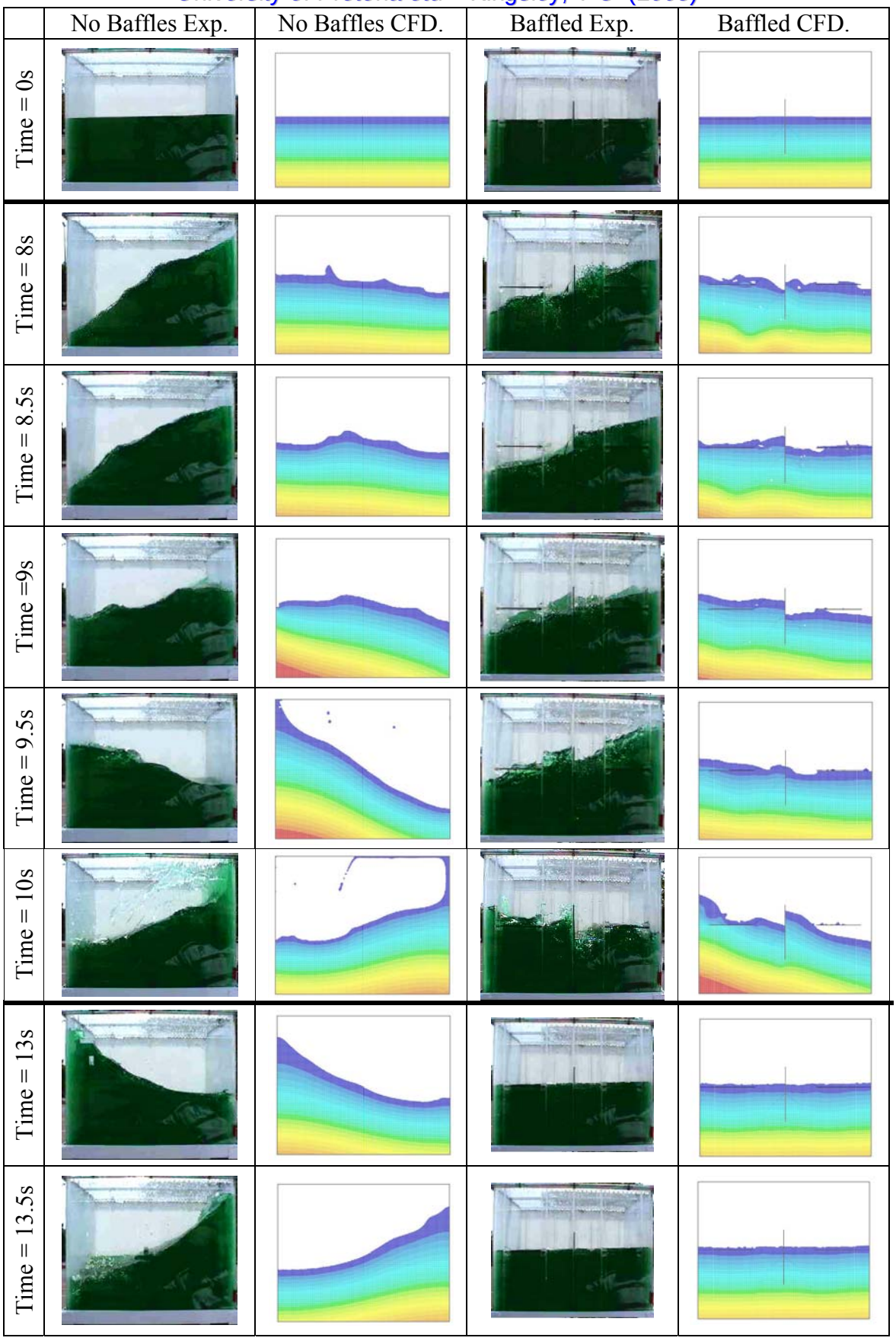

Figure 3.15: Comparative frames of liquid motion for CFD and experimental models (50% fill level)

The experimental pressure signal is converted according to a previously performed static calibration test. All data, both CFD and experimental, are again low-pass filtered at 5Hz. Variations in initial pressure levels (too high a pressure measured by the diaphragm of the transducer) is thought to be due to dithering, an effect caused by higher frequency excitations induced by the vibrations of the vehicle's moving mechanical parts (e.g., engine, gearbox). The baffled case clearly illustrates the very similar flow trend but differing amplitudes between the experimental and CFD results. This may be in part due to the deficiencies of the piezo-crystal linear accelerometer at low frequencies. The no-baffles case does not suffer as much from the variation in amplitudes since the waves are more often constrained by the lid of the container, i.e., the hydrostatic head cannot increase beyond the height of the tank. The water in the CFD model forms a lower slope against the wall than in the experiment, implying that the hydrostatic pressure in the experiment is maintained longer at the maximum head value than in the CFD model for the 7-10 sec time frame.

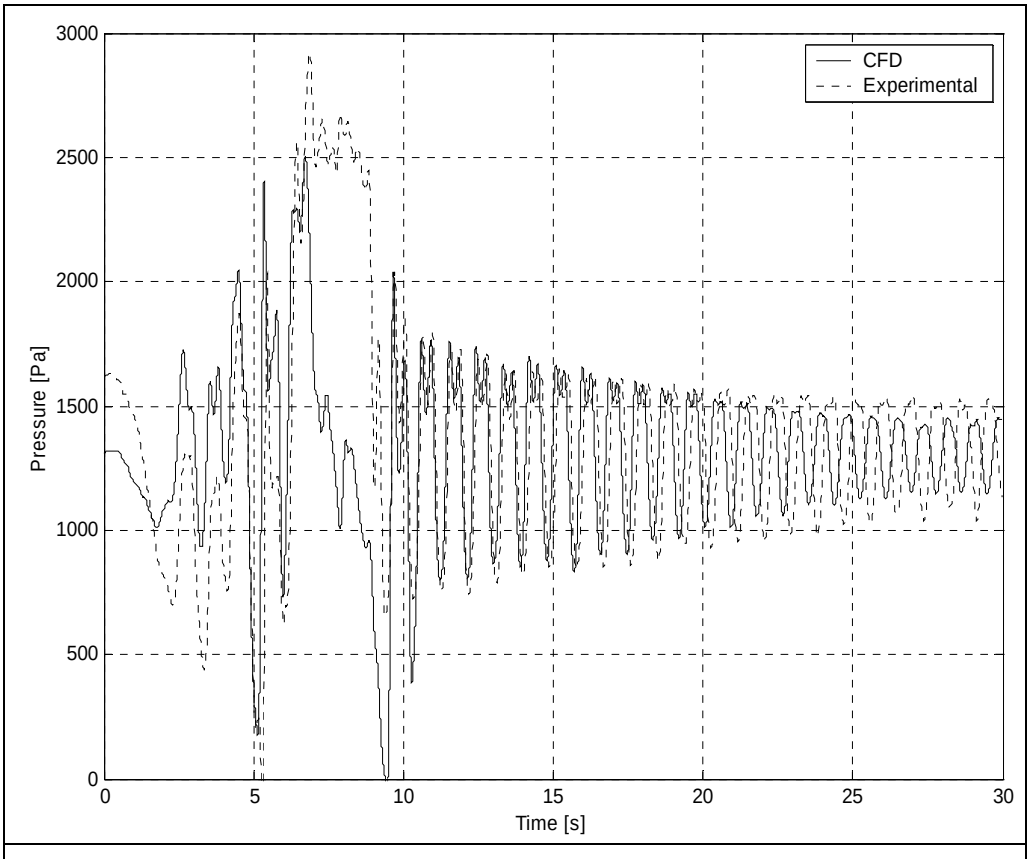

Pressure point P1 (No baffles case)

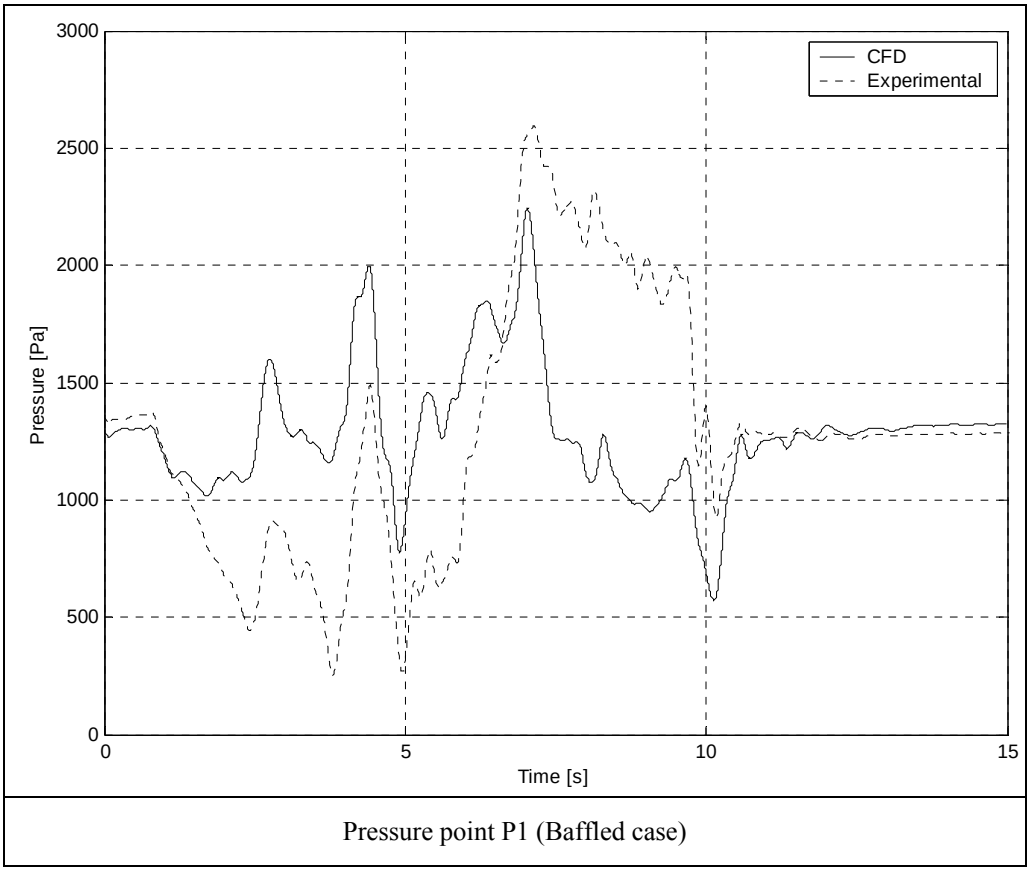

Figure 3.16: Comparative gauge pressure plots for the experimental model and the CFD

The above data can be further processed and compared from a pressure spectral density perspective. All pressure signals are passed through a Fast Fourier Transform and converted from the time domain to the frequency domain. Figure 3.17 below illustrates these data for the four cases in question (CFD and Experimental for baffles and no baffles), with spectral density (Pa^2/Hz) on the vertical axis and frequency on the horizontal axis. Also shown are the 1st two odd oscillatory modal frequencies based on linear flow theory [14]. The no-baffle case shows excellent agreement between the CFD and experimental model, while the baffled case once again shows agreement in the flow trend but a variation in amplitude. The 1st two odd oscillatory model frequencies are very closely captured, although the damping for the baffled case has removed the 2nd odd mode content. It should be noted that the magnitude of the low-pressure section of the signal will be higher for a lower amplitude wave. Both plots show the error in the 8 to 10 second range as low frequency (<0.5Hz) variations in amplitude.

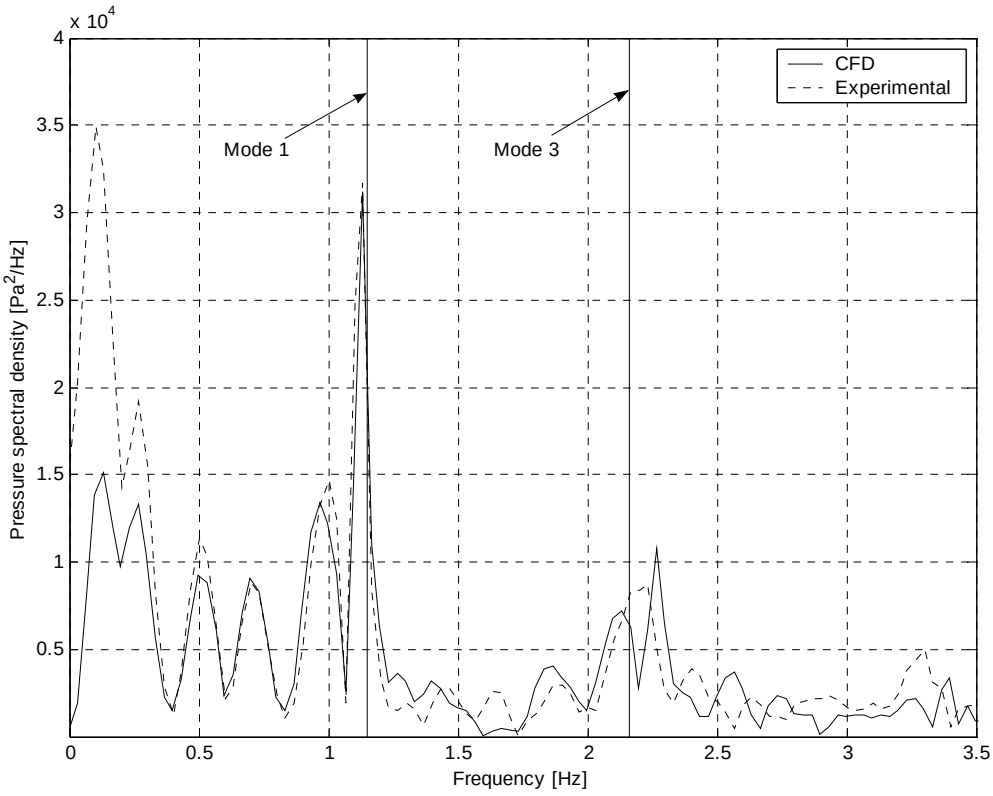

Pressure point P1 (No baffle case)

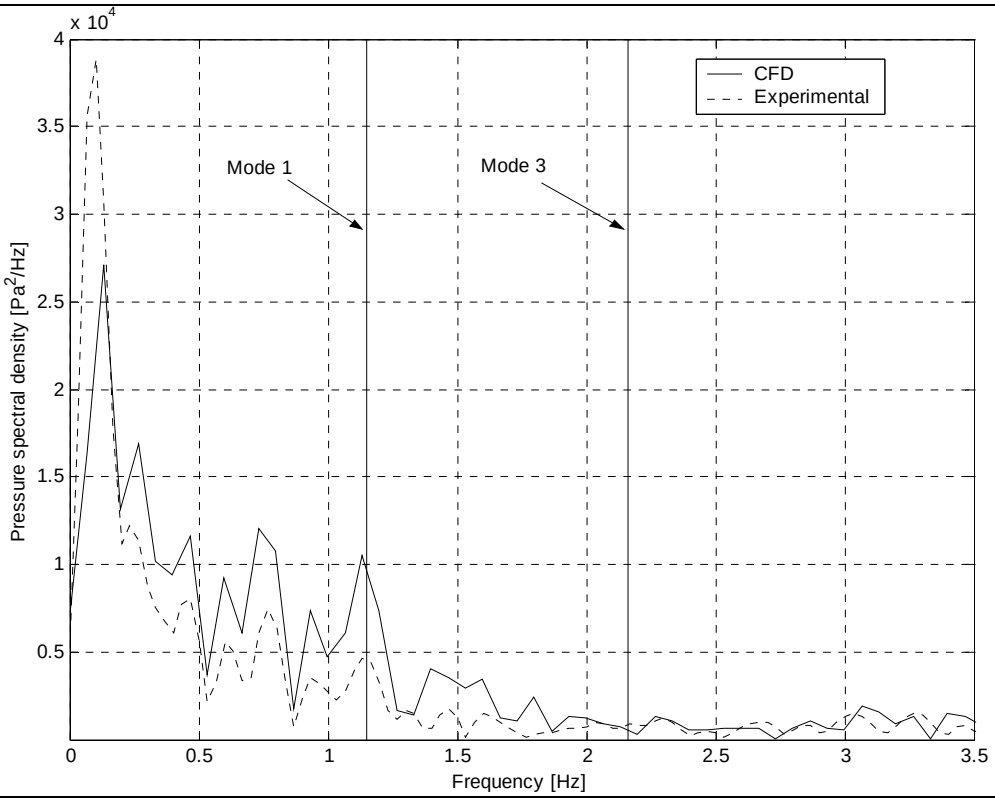

Pressure point P1 (Baffled case)

Figure 3.17: Comparative amplitude/frequency domain plots of pressure signals

3.3.3 Conclusion

Within the spectrum of this study, the results achieved are generally very acceptable. The validation study provides sufficient insight into the validity of the numerical model as well as some level of insight into the phenomenon of sloshing itself. The un-baffled case also provides additional and more interesting data about the oscillatory modes. Certainly within a design perspective, an improved numerical model would seemingly translate to an improved physical design.